J. Fluid Mech. (2004), *vol.* 501, *pp.* 303–326. © 2004 Cambridge University Press
DOI: 10.1017/S0022112003007560 Printed in the United Kingdom

A note on charged capillary jet breakup of conducting liquids: experimental validation of a viscous one-dimensional model

By J. M. LÓPEZ-HERRERA AND A. M. GAÑÁN-CALVO

Grupo de Mecánica de Fluidos, E.S.I, Universidad de Sevilla,
Camino de los Descubrimientos s/n 41092 Spain

(Received 24 March 2002 and in revised form 7 October 2003)

Controlled charged capillary jet breakup of conducting liquids with different viscosities and applied voltages are experimentally analysed in this work. Careful measurements of droplets size and charge transported by the main and satellite droplets have been carried out. The experimental results are compared with those obtained by an augmented one-dimensional Lee model (López-Herrera *et al.* 1999). Theory and experiments show a remarkable agreement, which validates the rather inexpensive one-dimensional models as suitable predicting tools for scientific and engineering applications from electrospraying to charged jet printing over other sophisticated, more expensive three-dimensional models. Our results show that satellite droplets tend to undergo Coulombic rupture even in the case of very moderate electrification levels when the Ohnesorge number is sufficiently large.

1. Introduction

As technological applications become increasingly demanding on aerosol quality and control on the droplet size and its homogeneity, the aerosol generation process itself is becoming one of the most widely and deeply analysed issues of fluid dynamics with free surfaces. In particular, the analysis is being increasingly focused on the capillary jet or liquid ligament dynamics as the inherent precursor of the droplet stream. Thus, emerging technologies to produce extremely controllable and high-quality liquid micro-jets, either by mechanical or electrical means, are now the subject of great interest in technological applications demanding very small and homogeneous droplet size. In general, the characteristics of an ideal, high-quality aerosol for a demanding application are naturally met by the aerosol resulting from the axisymmetric capillary breakup (Rayleigh breakup) of a number of small and steady liquid ligaments into droplets. In fact, when the conditions for this breakup regime are met, the spray quality is optimal since the droplet size is mainly uniform and it can be precisely controlled (droplet size is proportional to the jet diameter in this regime). For example, in so-called cone-jet electrospraying (Zeleny 1917; Cloupeau & Prunet-Foch 1989), the extremely thin steady liquid ligament formed and ejected by electrohydrodynamic forces breaks up into rather homogeneous-size charged micro- or nano-droplets, yielding a particularly high-quality aerosol (see for example Rosell-Llompart & Fernandez de la Mora 1994; De Juan & Fernandez de la Mora 1997*a*, *b*; Gamero-Castaño & Hruby 2002) when the liquid flow rate (or the liquid electrification level) is held below a certain threshold value.

In general, when electrostatic forces are used to assist the liquid jet formation or breakup, the control of the resulting spray involves the quantification of the size and charge of the droplets generated.

Most of the vast available literature on capillary jet breakup deals with non-charged jets. Available linear analyses (Rayleigh 1878; Weber 1931; Chandrasekhar 1961; Tomotika 1935 etc.) allow to be estimated the most probable resulting droplet size but they do not give any information on either the satellite droplets or the effect of the initial amplitude of the perturbation on the breakup process. Using perturbation schemes, more recently some authors have included nonlinear effects (Yuen 1968 or Chaudhary & Redekopp 1980 among others), explaining the appearance of the satellite droplets from the growing of higher harmonics of the initial perturbation. So far, analytical approaches have been unable to provide the interface position at the last stages of the breakup and, in consequence, cannot predict the volumes of the main and satellite droplets with enough accuracy.

Even with the axisymmetric simplification, the resolution of the Navier–Stokes equations in the presence of charges at a free boundary is not trivial. Using the jet slenderness, several one-dimensional models have been developed with notable success. Melcher & Warren (1971) employ this simplification for the first time in a model describing a jet in an imposed electric field, in the radial and axial directions. Other one-dimensional models such as the inviscid Lee model (Lee 1974), the Cosserat model (Green 1976) or the viscous Lee model (Eggers & Dupont 1994; García & Castellanos 1994) have been derived to deal with the time-evolving nonlinear jet dynamics towards breakup. For example, Ambravaneswaran, Phillips & Basaran (2000) analyse with great success the dripping faucet problem using a hydrodynamic one-dimensional model. A review and detailed derivation of the models available in the literature can be found in García & Castellanos (1994). Furthermore, direct simulations of the jet breakup using three-dimensional axisymmetric Navier–Stokes equations have been recently accomplished. For example, Keunings (1986) solves the breakup of non-Newtonian fluids, Ashgriz & Mashayek (1995) report numerical result on the breakup of a viscous jet, whereas Mansour & Ludgren (1990) simulate the breakup of an inviscid jet using a velocity potential formulation.

Most early experiments on the breakup of uncharged jets seek to compare and validate the results of the linear analysis, and to provide the resulting volumes of main and satellite droplets (Donnelly & Glaberson 1966; Goedde & Yuen 1970). For their application to ink jet printers, other experiments analyse satellite droplet formation and propose methods to eliminate them (e.g. by jet excitation with combinations of harmonics, Chaudhary & Maxworthy (1980) or Brenn & Lackermeier (1997) among others, or by the use of novel actuators (Barbet 1997)).

Most early published literature on electrically charged jets deals with linear analysis, considering the fluid as a perfect conductor. This provides dramatic simplifications in the calculation of electrical stresses on the jet's surface (the charge is distributed on the surface only, and the electric field is normal to it). Basset (1894) studies this configuration by a linear analysis and shows that, for an axisymmetric breakup, the electric field stabilizes the long-wavelength perturbations and destabilizes the short ones. Melcher (1963) shows that, for a moderate electrification (moderate electric stresses compared to surface tension forces), the faster growing mode is always the axisymmetric one. Saville (1971*b*) performs a linear analysis of a conducting liquid, adding the effect of liquid viscosity. Some other linear analysis show that a tangential electric stress can attenuate the growth of perturbations, promoting very long jets such as those obtained in an electrospray using moderate

viscosity liquids in the non-whipping jet regime (Saville 1970; 1971*a*; Mestel 1994, 1999).

Nonlinear studies are less common in the literature. Setiawan & Heister (1997) analyse the three-dimensional, axisymmetric breakup of an inviscid conducting jet under high electrification levels, and find that it is possible to form Taylor-type cusps on the jet surface. López-Herrera, Gañán-Calvo & Perez-Saborid (1999) tackle the problem of a viscous jet, using the one-dimensional Lee model. They focus their attention on the resulting charge and volume distribution between the main and satellite droplets.

Experimental work on electrified jets starts with Magarvey & Outhouse (1962). The breakup is not forced in that work, and the control parameters are the flow rate and the applied voltage. They experimentally report the transition from axisymmetric to whipping breakup as the voltage is increased. Huebner (1969) shows how the main droplet size decreases as the voltage increases.

Other drop formation phenomena under the influence of electric fields such as liquid dripping from capillary tubes or the breakup of liquids bridges subjected to a great variety of electrical and mechanical conditions have been the subject of extensive experimental (Zhang & Basaran 1996) and theoretical studies (either analytical or numerical, e.g. Notz, Chen & Basaran 2001), when viscous forces are small or negligible in the breakup dynamics, and when electrical relaxation times are negligible compared to the characteristic hydrodynamic times of the process. Those detailed and incisive studies may be relevant to drop formation from a liquid jet or column breakup as long as the boundary conditions allow a qualitative comparison, although it is hard to obtain general conclusions applicable for both cases. In particular, it is worth noting that Basaran's group's studies on this subject (e.g. Zhang & Basaran 1996; Notz *et al.* 2001; Wilkes, Phillips & Basaran 1999; Yildirim & Basaran 2001) allow an exhaustive and accurate analysis of the breakup, and in many cases of the pinch-off extremely close to detachment (Chen, Notz & Basaran 2002). In our work, however, we aim to study other processes and quantities of general interest such as: (i) the splitting mechanism of charges between the main and satellite droplets, (ii) the overall charge carried by those droplets, and (iii) their eventual electrohydrodynamic stability (e.g. how close are they to the Rayleigh limit charge). The accurate but expensive tools used in previous references are more than adequate for these tasks; thus, under sufficiently general conditions, a one-dimensional model such as that proposed in López-Herrera *et al.* (1999) yields excellent results (for a comparison on the suitability of either a three-dimensional axisymmetric or a one-dimensional model see for example Yildirim & Basaran 2001), which allows a detailed and quite inexpensive exploration of wide parametrical ranges of interest (wavelength, viscosity, surface tension and electrification levels).

The aim of the present note is twofold: (i) to present a large set of measurements from highly controlled experiments using a relatively simple set-up, where the role of both viscosity and electric forces relative to surface tension (i.e. the role of Ohnesorge and electrical Weber number, or Taylor number) in charged capillary jet breakup is investigated, and (ii) to compare these results with predictions from a simplified model with a quasi one-dimensional approximation (Lee's model) for the jet hydrodynamics. Consistently with other previous works using this approximation to solve hydrodynamic, axisymmetric, slender problems, where bulk forces are approximated very well, we show the predictive capabilities of our model if that bulk force calculation is combined with a sufficiently accurate calculation of the existing stresses on the surfaces (both mechanical and electrical in our case).

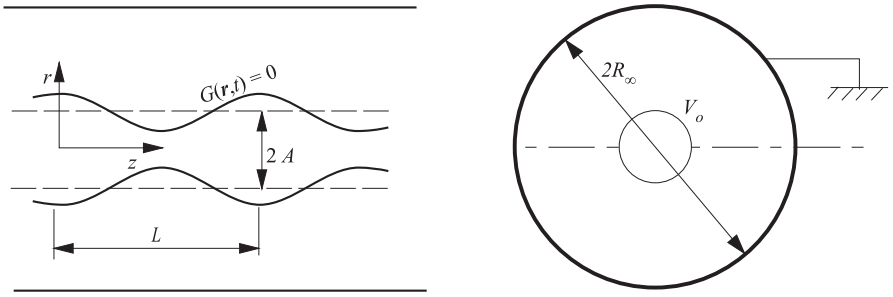

FIGURE 1. Geometrical configuration and electric potential values at the surfaces of interest.

2. Theoretical model

2.1. *Geometrical configuration*

When a capillary jet of a Newtonian, homogeneous liquid moves with velocity such that capillary waves are convected downstream, its dynamical evolution can be described with sufficient accuracy by a Lagrangian-type framework (Keller, Rubinow & Tu 1973), i.e. by a model considering the temporal evolution of a portion of the jet only. As is well-known, the errors incurred in the assumption of periodicity are related to the ratio between the convective and the breakup times. In fact, the differences between adjacent portions of the evolving real jet are due to *convection*, whose characteristic associated time is $t_v \sim L/U$, where L and U are the perturbation wavelength and the average liquid velocity in the intact jet sufficiently downstream of the exit orifice. Furthermore, the dynamic evolution by capillary forces is associated to the capillary time $t_c \sim (\rho A^3/\gamma)^{1/2}$, where ρ, γ, and A are the liquid density, surface tension, and the intact jet radius, respectively. Thus, non-periodicity involves errors of the order of $t_c/t_v \sim (\rho A^3 U^2/(\gamma L^2))^{1/2} \lesssim (\rho A U^2/\gamma)^{1/2} = We^{1/2}$, since we will always consider in this work $A \lesssim L$. Errors are small for Weber numbers $We = \rho A U^2/\gamma \gg 1$. When the Weber number exceeds a critical value, however, either the non-symmetric perturbations grow faster than the axisymmetric ones or the influence of the surrounding atmosphere becomes not negligible. Since our interest is focused on the even, axisymmetric capillary jet breakup because of its importance in most applications where a high-quality spray is needed (i.e. in electrospray for small liquid flow rates, when the highest-quality aerosol is obtained), we restrict our study to moderate We (smaller than about $We \sim 500$ in our conditions, see Sterling & Sleicher 1975). Additionally, though, we consider We values sufficiently larger than unity (larger than about $We \sim 30$) and, accordingly, we use a Lagrangian description following the evolution of a jet portion only (see figure 1). Although this We range may seem quite narrow, it nevertheless strictly coincides with the range of highest droplet size homogeneity of interest in applications.

As can be observed in figure 1, the shape of the liquid column can be defined by the implicit function,

$$G(\mathbf{r}, t) = 0 \quad \text{or, explicitly,} \quad r = F(z, t), \tag{2.1}$$

where r, z, and t are the usual radial, axial and temporal dimensional coordinates. Figure 2 illustrates the accuracy of the Lagrangian description and the one-dimensional model used in this note (and proposed in López-Herrera *et al.* 1999) by comparison to a real breakup from one of the experiments performed in this work. Figure 2(*b*) has been composed by selecting symmetrical frames obtained from the

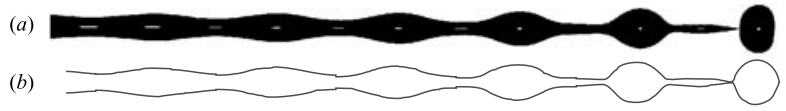

FIGURE 2. (*a*) Axisymmetric breakup of a weakly electrified jet from our experiments compared to (*b*) the corresponding numerical simulation using our periodic augmented one-dimensional model; (*b*) is generated by the superposition of 6 frames (numerically calculated) separated by a time step equal to L/U.

temporal evolution computation in time intervals equal to one wavelength divided by the convective velocity of the jet. In this composition, an inevitable small step-discontinuity in the necking/swelling regions corresponding to the symmetrical frame borders can be noticed, though resulting from a simple step-like conversion from Lagrangian to spatial descriptions. These small steps can be smoothed out by an appropriate small linear temporal correction in the spatial, axial direction along every jet portion (however, since figure 2 is simply for illustrative purpose, this additional refinement is nonsensical and may be misleading).

2.2. *Forces on the jet and the one-dimensional model*

In our experimental conditions, surface tension, density and temperature gradients are considered absent. The mechanical interaction between the jet and the surrounding ambient can be considered negligible, as can the acceleration along the jet resulting from external forces such as gravity or tangential stresses of any nature. This last assumption is valid as long as the increment of the kinetic energy along a wavelength L is negligible compared to its local average value,

$$\frac{\rho U \Delta U/L}{\rho U^2/L} \sim \frac{\Delta U}{U} \ll 1 \tag{2.2}$$

where U is the average axial liquid velocity. Since the increment of velocity ΔU due to gravity g along a wavelength L is of order $\Delta U \sim \sqrt{gL}$, the restriction (2.2) is equivalent to considering that the Froude number, defined as $Fr = gL/U^2$, is much smaller than one. Under these conditions, mass and momentum transport between adjacent portions of the jet followed by the Lagrangian description are negligible.

Even under the simplifications described above, the resolution of the Navier–Stokes equations with non-trivial boundary conditions at free surfaces becomes a computationally expensive task. As we will show here, the introduction of a one-dimensional approximation in the hydrodynamic model drastically reduces computational efforts with little accuracy loss. Many different models have been derived with notable success (e.g. Lee 1974; Eggers & Dupont 1994; García & Castellanos 1994 among others). In this work, we aim to show that the viscous Lee model, derived by Eggers & Dupont (1994) and García & Castellanos (1994) simultaneously, with the addition of electric field effects (López-Herrera *et al.* 1999), is a tool particularly well-suited to analyse the charged liquid jet dynamics. The equations of the model, made non-dimensional with the intact jet radius A, the capillary time $(\rho A^3/\gamma)^{1/2}$, the liquid density ρ and the electric potential $E_{no}A$, (where E_{no} is the normal electric field on the intact jet surface), are

$$(f^2)_t + (f^2 w)_z = 0, \tag{2.3}$$

$$f^2(w_t + w w_z) = -f^2(p_{ce})_z + 3C(f^2 w_z)_z, \tag{2.4}$$

$$p_{ce} = \frac{1}{\left(1 + f_z^2\right)^{3/2}} \left(\frac{1 + f_z^2}{f} - f_{zz} \right) - \Gamma_o \left(1 + f_z^2\right) (\phi_r)^2, \tag{2.5}$$

$$\frac{1}{r} (r\phi_r)_r + \phi_{zz} = 0, \tag{2.6}$$

with boundary conditions

$$\left.\begin{aligned} w(z = 0, t) = w(z = \lambda, t) = 0, \\ f_z(z = 0, t) = f_z(z = \lambda, t) = 0, \\ \phi_z(r, z = 0, t) = \phi_z(r, z = \lambda, t) = 0, \\ \phi(r = (R_\infty / A), z, t) = 0, \end{aligned}\right\} \tag{2.7}$$

where as usual r, z, and t are the radial, axial and temporal non-dimensional coordinates, respectively; w, f are the non-dimensional averaged axial velocity and non-dimensional jet radius, respectively; p_{ce} is the capillary plus electrical pressure; and $\lambda = L/(2A)$ is half the non-dimensional wavelength. The relevant parameters of the problem are the Ohnesorge number given by $C = \mu/(\rho\gamma A)^{1/2}$ and the Taylor number given by $\Gamma_o = \varepsilon_o A E_{no}^2/(2\gamma)$, where ε_o and μ are the electric permittivity of vacuum and liquid viscosity, respectively. In practice, we apply a certain potential difference V_o between the intact jet and a concentric cylindrical electrode of radius R_∞ (see figure 1), and compute E_{no} as the relevant parameter that fixes the jet's electrification level and the surface charge density on the intact jet.

At this point it should be noted that an electrical boundary condition should be added to those of (2.7) in order to close the problem formulation properly. A careful discussion on electric charge conservation must be undertaken before the choice of this lacking boundary condition.

2.3. *The electrical problem*

In this work we aim to describe charge evolution in the capillary jet breakup problem when this charge is basically confined on the liquid surface. The jet charge is induced by applying a potential difference between the liquid jet and the electrode which surrounds the jet (figure 1). The real charged jet issues from a liquid source, where the voltage is applied, and ends up in the breakup region as a jet locally (but not globally) periodic for a constant imposed jet velocity.

We aim to compare this charged real jet breakup with a model which assumes an infinitely long and spatially periodic capillary liquid column. The comparison is consistent under the conditions that we will discuss in the following. First, the boundary conditions and charge conservation requirements needed to close the electrohydrodynamic spatially periodic problem (every wavelength portion evolves identically and simultaneously) involve an indeterminacy which demands a careful discussion for our theoretical periodic infinite domain. Consider a column with length L_j of a liquid with an electrical conductivity K. This liquid column can be thought of as a resistor with value $\Omega = L_j/(K\pi A^2)$. Obviously, in the limit of an infinitely long jet, its resistance would be infinite for any arbitrary finite value of the liquid conductivity, unless we assume that the liquid is a perfect conductor (infinite conductivity), for which the total liquid column resistance would be undetermined. Bearing in mind this conceptual indeterminacy, we thus have the freedom to adopt two possible limiting electrical conditions, discribed below when the proposed model is compared to a real situation.

2.3.1. *Imposed potential*

Under the assumption that the liquid is a perfect conductor, a limiting situation is that the liquid column resistance is zero. In this case, its surface electric potential ϕ_o is equal to that at both jet ends, at infinity, which can be maintained constant during the time evolution of the jet. Therefore, the boundary condition

$$\phi(r = f(z, t), t) = \phi_o \tag{2.8}$$

should be added to the set of conditions (2.7) for the completeness of the model.

In this case, since the liquid surface evolves in time and we keep the surrounding electrode at a fixed position, the surface charge of every wavelength portion of the jet must slightly change, according to the changing geometry and the imposed potential, which would require a non-zero charge circulation along the jet. This would not represent a problem for a truly perfect conductor at any time up to the final instant when the last liquid molecules or atoms split apart at pinch-off.

2.3.2. *Charge conservation*

However, all real liquids exhibit a finite electrical conductivity. In this case, the liquid column resistance would be infinite and thus, since no charge can be supplied from infinity, the total surface charge of a wavelength portion of the jet must be conserved. The liquid surface electric potential will therefore take an appropriate value at every moment consistent with its instantaneous geometry and boundary conditions, assuming that the surface portion of the jet must be equipotential at each instant. Thus, the total charge on a wavelength portion of the jet must satisfy

$$q_T = \int_o^{2\lambda} e_n f \left(1 + f_z^2\right)^{1/2} \mathrm{d}z = 2\lambda. \tag{2.9}$$

It should be stressed that this case is perfectly compatible with the assumption of an almost perfect local conductor, from the point of view of the local evolution of a single jet portion, if the characteristic charge relaxation time $t_e \sim \varepsilon/K$ is much smaller than the characteristic time of fluid motion given by the capillary time t_c, which is a required condition to assume surface equipotentiality at each wavelength. In fact, for our infinite, periodic model it is worth noting that independently of the general requirement $t_c \gg t_e$ for a local quasi-perfect conductor assumption, charge supply from the far ends of the jet involves arbitrarily large resistance values.

We are thus left with two possible limiting formulations for the electrical problem: one can impose either (i) a constant surface electrical potential along the whole breakup process, or (ii) the conservation of total surface charge on a wavelength portion of the jet.

It is worth noting however that both formulations coincide when one connects both ends of the jet at infinity and assumes that the surrounding concentric electrode is an infinite torus which isolates the jet from the universe. This is a consistent corollary since the potential at infinity can be changed in time at will (the charge conservation condition is obviously a particular case of the imposed potential when it follows the appropriate temporal law, see figure 3*b*).

2.3.3. *Model closure and consistency*

A real capillary jet issues from a liquid source and ends up in the breakup region, in which a liquid particle will enjoy a residence time in the jet given by the growth time of perturbations (proportional to t_c). Thus, free charges are relaxed on the surface along the jet if $t_c \gg t_e$, which means that the inner electric field should vanish. This

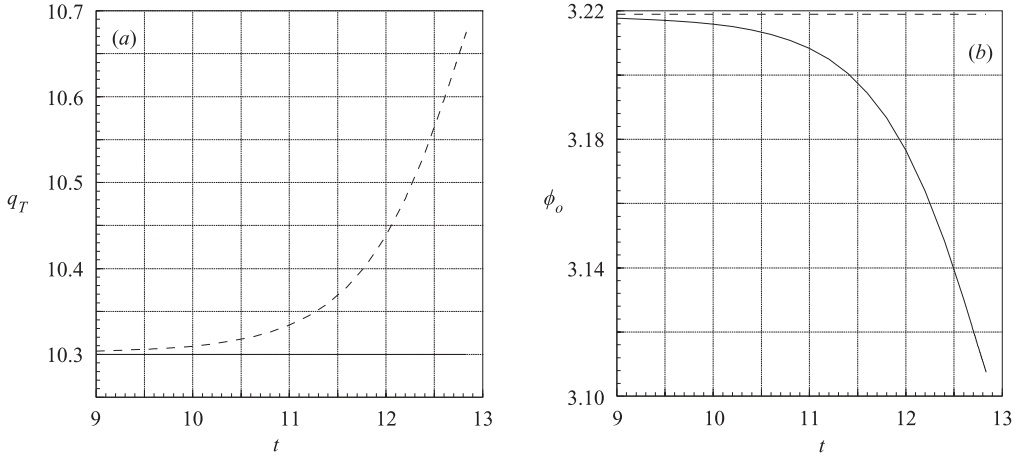

FIGURE 3. Evolution close to pinch-off of (*a*) total surface charge of a of the jet wavelength portion, and (*b*) surface potential, using the charge conservation condition (—) and equipotentiality condition (- - -).

is compatible with the condition of equipotentiality (equation (2.8)), if the amount of charge per unit time withdrawn by the detaching droplets coincides with the current convected by the jet surface, since there is no need for a further supply of charge by conduction driven by inner electric field. Paradoxically, this is also compatible with the alternative charge conservation condition (equation (2.9)).

In reality, the paradox arises through an inappropriate extension to the limit of logical reasoning based on small quantities. Our real jet is almost but not perfectly periodic in space, our real jet is very long but not infinite, and our liquid is almost but not perfectly conducting. Here we suggest a simple way to avoid what may turn into a kind of over-subtle Byzantine discussion: to embrace a perfectly periodic, perfectly conducting model and test both equipotential and charge conservation conditions. If the differences found in the results are smaller than the errors incurred in assuming the perfect periodicity or ideal conducting limits from a real jet, then a further discussion on the issue of what is the appropriate closing condition is pointless when making comparisons between model and experiments.

In figure 3, we show the evolution of both the total surface charge of a jet wavelength portion and the surface potential using both surface charge conservation and equipotentiality conditions for a typical case ($\lambda = 5.15$, $C = 0.128$ and $\Gamma_o = 0.389$). Departures are only noticeable very close to pinch-off, and the maximum errors found are of the order of less than 4% (obviously, the main reason for this small discrepancy is the liquid domain slenderness). Since the errors incurred in assuming periodicity, of the order of the inverse of the square root of the Weber number, are even larger than those, then we can consistently close our model with either one or the other condition.

We have chosen charge conservation since it results in a slightly smaller error when the numerical results are compared to experiments. Additionally, we should note that charge conservation is the most mathematically sound condition for our model under the considerations previously given for an infinite isolated jet both ends of which are connected at infinity.

A detailed derivation of the equations and resolution methods can be found in López-Herrera *et al.* (1999). Our aim here is to perform a careful experimental assessment of the model already presented and its assumptions.

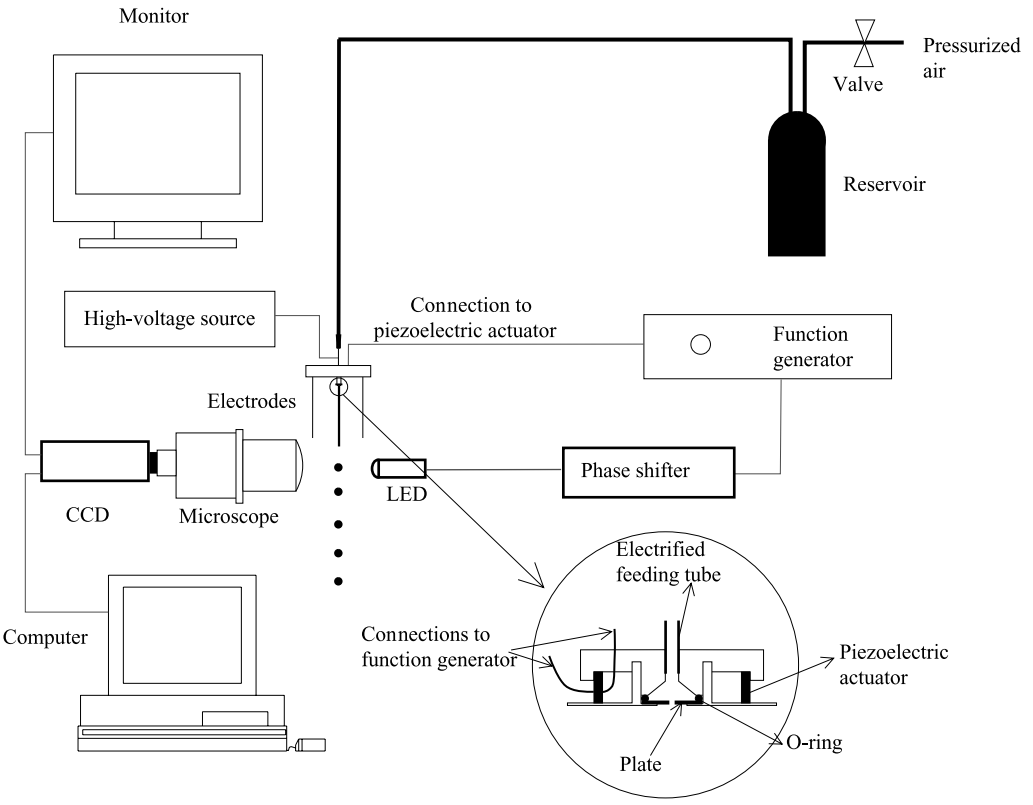

FIGURE 4. The experimental set-up with a detail of the injector.

3. Experiments

Our experimental set-up is aimed at the precise measurement of both the charge transported by the droplets and their size as functions of the physical properties of the liquid and control parameters in our experiments.

Liquid contained in a reservoir is forced through a carefully made round-shaped orifice with diameter of 400 μm to obtain a clean, laminar jet with a radius very close to 200 μm. The liquid is forced with velocities ranging from 3 to 5 m s^{-1}, for which we obtain a plug-flow velocity within a few millimetres from the exit orifice in our experimental conditions. We impose a continuous sinusoidal perturbation on the jet by forcing the plate containing the exit orifice with a piezoelectric actuator (a Pz-27 tube from FERROPERM) driven by a function generator (PM-5135 Philips function generator). The actuator is located sufficiently close to the orifice (see figure 4) to overcome any surrounding noise. The mechanically perturbed jet then breaks into droplets following a highly reproducible, controlled process. Using classical stroboscopic techniques, where a light source is pulsed at the same frequency as the jet perturbation, the jet breakup can be easily monitored in its greatest detail (see for example figure 5) by multiple imaging superposition, where many hundreds of single light strokes per image are recorded. The light source is a high-luminosity LED driven by an electronic circuit which transforms a TTL signal from the function generator into a train of pulses of 700 ns width and the same frequency as the excitation. Also, the electronic circuit can produce a controllable phase shift with respect to the excitation, which allows a detailed pseudo-slow-motion 'video-edition'-like study

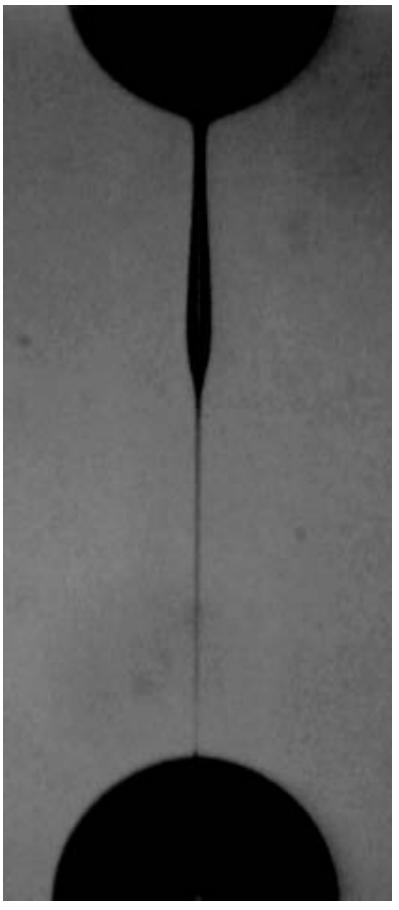

FIGURE 5. Image of the last stages of the breakup of an uncharged highly viscous jet (liquid: propyleneglycol) as obtained with our stroboscopic set-up and a conventional CCD camera (25 f.p.s., not a high-speed camera).

(forwards or backwards) of the jet breakup when the phase shift is slowly changed with time. The images, magnified with a microscope, are stored in a PC.

At the location downstream of the exit orifice where the jet breakup phenomena are recorded, the liquid velocity (typically 4 m s^{-1}) is large compared to that due to gravity alone. In other words, the Froude number gL/U^2 in our experiments is of the order of 10^{-4}, for which the acceleration due to gravity can be neglected. Consequently, the jet can be considered virtually cylindrical before the breakup region. The dynamical Weber number is typically $We \sim 100$. Thus, convective velocities are about $We^{1/2} \sim 10$ larger than the capillary liquid jet breakup velocities, which means that our model periodicity assumptions are correct within errors of the order of $We^{1/2} \ll 1$.

For the purposes of a quantitative comparison with our theoretical model, in this work we wish to electrify the jet in such a way that the tangential electric field is zero. Therefore, in order to minimize the appearance of any possible voltage drop along the jet, we place two parallel metallic plates of 40 mm width and 155 mm long in the direction of the jet's axis at a distance of 20 mm from the jet (see figure 4), and apply a high voltage difference (high voltage source Bertran model 205B-10R) between the exit orifice and the parallel plates. The jet flow is equidistant from the parallel plates.

Liquid	γ (N m^{-1})	ρ (Kg m^{-3})	μ (c.p.s.)
Low-viscosity mixture (L)	0.0451	1100	8
Medium-viscosity mixture (M)	0.052	1116	14
High-viscosity mixture (H)	0.0461	1124	28

TABLE 1. Relevant physical constants of the liquids employed.

In addition, in this work we are interested in phenomena where electrical relaxation effects are negligible, which demands small electric times $t_e \sim \varepsilon K^{-1}$ compared to the capillary ones $t_c \sim (\rho A^3 \gamma^{-1})^{1/2}$. The liquid conductivities used are of the order of $K \sim 10^{-3}$ S m^{-1}, whereas the relative permittivities $\beta = \varepsilon/\varepsilon_o$ are approximately equal to 60. Therefore, in the present experiments the ratio t_e/t_c is of order of 10^{-4} and the jet can be considered equipotential. Consequently, the liquid jet can be considered virtually free of any tangential electric stress, the drop voltage along the jet can be assumed negligible and, finally, the liquid conductivity and permittivity disappear as relevant physical properties of the problem.

3.1. *Measurement of the physical properties and the jet velocity*

Three mixtures of water and glycerin have been used in this study to cover a significant range of viscosities. Surface tension have been measured with a digital tensiometer Krüss K10T, the viscosity with a Brookfield Digital viscosimeter model DV-E, and the density with a precision balance (Scout Ohaus), in a controlled temperature environment (22 °C). Values are summarized in table 1.

In order to achieve a good control of the liquid viscosity, this parameter was measured before and after an experimental series is recorded. On the other hand, it is worth noting that our liquid surface tension measurements are smaller than those expected using mixtures of pure liquids (Lide 1990). This may be due to the use of filtered tap water, but this is of a minor importance for our purposes since we are interested in using liquids with accurately measured physical properties (density, viscosity, surface tension, electrical conductivity and permittivity) under controlled temperature conditions, instead of liquids with perfectly controlled chemical composition (purity, concentration, etc.).

The wavelength is directly measured from the acquired images. In practice, an average measurement of the wavelength L is made along the jet to maximize experimental accuracy. The liquid velocity U of the intact jet, or the average velocity of a jet portion with length L, can be simply calculated from the frequency of drop formation F (equal to the excitation frequency in our global periodic conditions) as

$$U = LF, \tag{3.1}$$

which is valid under the hypothesis that the drop does not undergo axial accelerations.

3.2. *Droplets and jet radius measurement*

The jet and droplet shapes are measured by image processing with a commercial program (Corel Photo Paint 9.0) which transforms the 256 grey image to a black and white image for easier interface detection and shape digitization (see figure 6). Under the working conditions, the grey scale and grey border level for profile detection can be adjusted using a calibrated glass filament of known diameter. We have used a resolution of 5 microns per pixel in this experimental work.

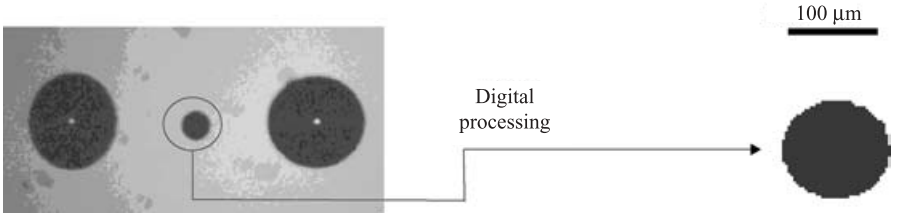

FIGURE 6. Digital shape processing is optimized using the more critical, smaller droplet image. Image resolution is 5 microns per pixel.

The intact jet radius measurements give 198 μm, 206 μm and 210 μm for the liquids with 'low' (50/50 water volume/glycerol volume), 'medium' (40/60 water volume/glycerol volume) and 'high' (30/70 water volume/glycerol volume) viscosities employed, respectively, independently of the liquid flow rates and the axial point observed in our experimental range. These small variations from liquid to liquid may be due to wetting differences at the orifice edge.

The satellite droplet radius is calculated from a sphere of volume equivalent to that obtained by numerical integration of the acquired droplet image profile. In order to minimize the errors, each satellite droplet is photographed at several different axial positions and an average volume is calculated. Thus, the main droplet radius is easily and accurately calculated from the experimental parameters (measured jet wavelength and intact jet diameter) and the calculated satellite volume.

3.3. *Calculation of the surface charge density; determination of the Taylor number*

The Taylor number Γ_o, or the ratio of electric to capillary forces,

$$\Gamma_o = \frac{\varepsilon_o A E_{no}^2}{2\gamma}, \tag{3.2}$$

provides information about the 'jet electrification level'. This number must be determined from an accurate calculation of the surface charge on the jet, or the normal electric field at the intact jet surface E_{no}. The use of a cylindrical conducting electrode concentric to the jet prevents jet visualization, so we have used parallel plates to simulate the same final electrostatic effect on the jet. In order to assess whether the experimental electrode configuration can accurately approximate the concentric electrode configuration, we have used the boundary elements method (Brebbia & Dominguez 1989) to calculate the electric field on the jet surface for a given potential difference between the jet surface and the parallel plates. Note that since the width of the electrodes and the distance between them is much larger than the jet radius, the resulting electric field distribution on the jet surface is almost axisymmetric (see figure 7), with deviations smaller than 0.07% (7×10^{-4}), which justifies the use of our experimental set-up to simulate axisymmetric electrifying conditions on the jet. Thus, the average normal electric field on the surface due to a difference of 1 V between the jet and electrification electrodes gives $E_{no}(1\mathrm{V}) = 1.232 \times 10^3\ \mathrm{V\,m^{-1}}$, $1.178 \times 10^3\ \mathrm{V\,m^{-1}}$ and $1.161 \times 10^3\ \mathrm{V\,m^{-1}}$ for the intact jet radius of 198 μm, 206 μm and 210 μm, respectively. Therefore, the Taylor number in a particular experiment can be calculated by (3.2), where $E_{no} = E_n(1\mathrm{V}) \times V_o/1\mathrm{V}$ is the normal electric field at the intact jet surface and V_o is the voltage applied to the jet in volts (typically several kilovolts).

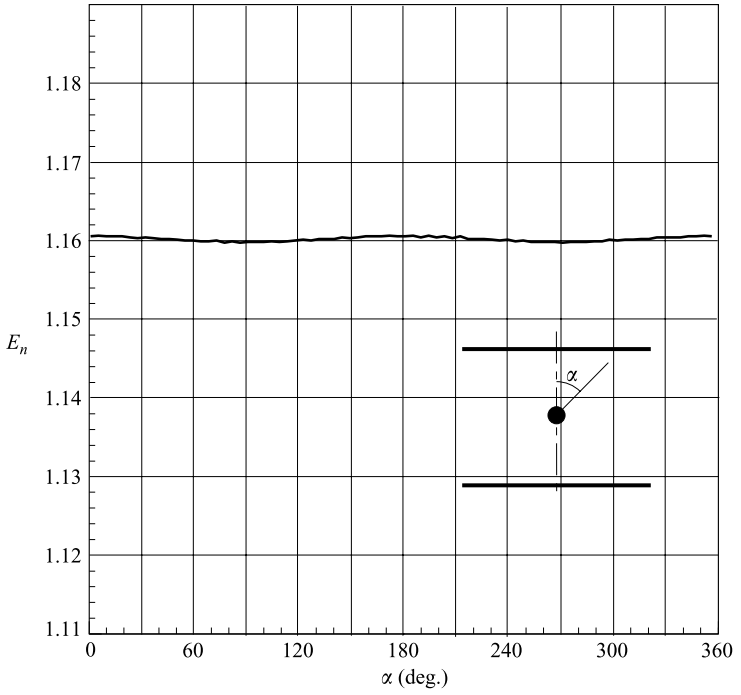

FIGURE 7. A realistic distribution of the normal electric field (in $V\,mm^{-1}$) on the intact jet surface in our experimental set up as calculated using a two-dimensional boundary elements method in the slice domain shown in the insert. Note the small deviations (smaller than a 0.07%) from a constant value corresponding to an axisymmetric configuration.

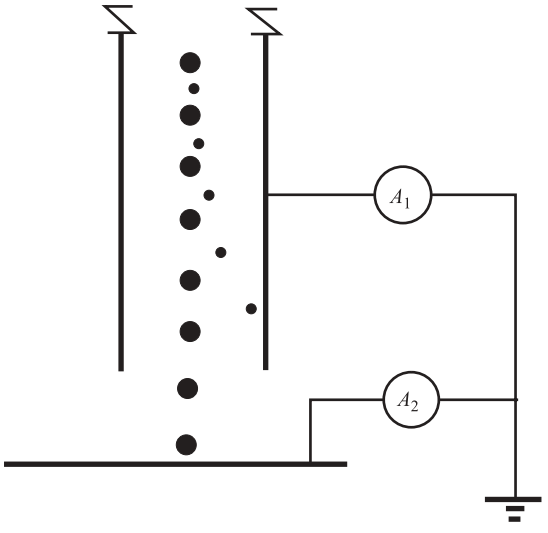

FIGURE 8. Discrimination of the charge transported by the satellite and main droplets.

3.4. *Droplet charge measurement*

The charge of each droplet can be calculated from the electric current transported and its volume. Two picoammeters are independently connected to the electrification electrodes and to a collector electrode located downstream (see figure 8), respectively.

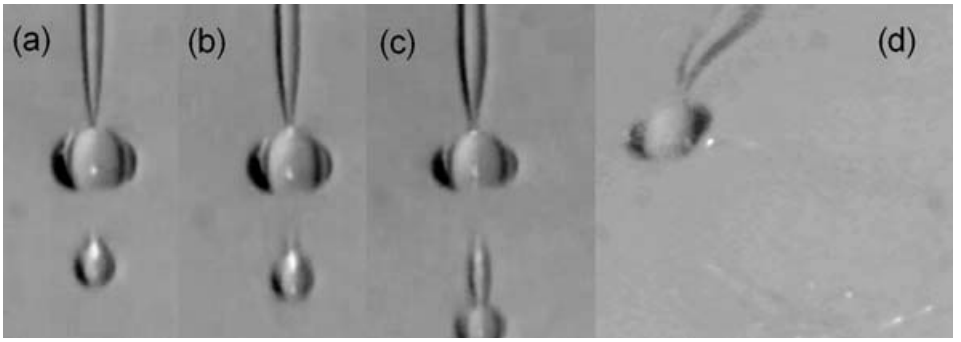

FIGURE 9. Instants of capillary liquid jet final breakup for several values of the electrification level. $C = 0.078$ in all cases. (*a*) $\Gamma_o = 0$, (*b*) $\Gamma_o = 0.234$, (*c*) $\Gamma_o = 0.651$, (*d*) $\Gamma_o = 0.938$. Note that these pictures do not correspond to consecutive steps of the same breakup event, but they correspond to the final instants of the jet breakup for different experimental conditions.

Thus, the electric current transported by the main and the satellite droplets can be independently measured since a natural segregation between the main and satellite droplets takes place along their trajectories: due to their smaller mass, the satellite droplets impinge on the electrification electrodes whereas the main droplets, whose trajectories are hardly affected, eventually impinge on the collector electrode. In order to assess how well our experimental set-up can discriminate between the charge on main and satellite droplets, based on the satellite segregation effect, we moved the plates along the jet axis in the upstream direction until the electric current reading of the picoammeter suddenly drops by some orders of magnitude, exactly when the observed satellites trajectories miss the plate where they where previously collected. In another assessment of the system, we intentionally intersected the satellite trajectories before they hit the collecting plate, and the same drop in the electric current reading as before is observed. The main or satellite droplet charge Q experimentally measured is then simply given by $Q = I/F$, where I is the corresponding electric current (main or satellite) and F is the excitation frequency.

In the model we compute the satellite and main droplet volumes and charges by calculating the integrals (2.9) and the volumes in domains $(0, z_{f_{min}})$ and $(z_{f_{min}}, \lambda)$ respectively, where $z_{f_{min}}$ is the axial coordinate where the neck radius is minimum.

It is worth of noting that once the velocity of the jet U is fixed, the total current measured by both picoammeters connected to either the parallel plates or the downstream collecting metallic funnel is independent of the excitation frequency (in other words, that $q_T \sim \lambda$, in accordance with charge conservation condition (2.9)).

4. Experimental results

Before proceeding further we would like to give an illustration of the effects produced by the jet electrification in our experiments. Figure 9 shows how the final instants close to pinch-off are affected for increasing electrification levels. Note that the different pictures do not correspond to the same breakup event (these are selected pictures of the last instants before pinch-off of a charged jet breakup from different experiments and for different electrification levels). Consistently with prior results from Cloupeau & Prunet-Foch (1989) (their figure 14, p. 152) for electrospraying, the effect of the electrification level on the main drop–satellite splitting at breakup is hardly noticeable or mild up to a limiting Γ_o value, which depends slightly on the

viscous parameter C. This point represents a more or less abrupt transition to an asymmetric breakup, where kink instabilities abruptly grow and Coulombic fissions take place (see in figure 9*d*). One of the aims of this note is to provide precise experimental and numerical data which show that, in the range of electrification levels and Weber numbers for which the breakup is axisymmetric, the nonlinear breakup process does not undergo other major significant alterations than a change in the breakup wavelength and frequency associated with the moderate change in the effective surface tension due to the presence of the electric field. Additionally, we will show that the resulting charge of the satellite is closer to the Rayleigh limit than that of the main droplet in all experimental conditions.

In this note, the experimental emphasis is on the size and charge of droplets. Other quantities of interest, however, such as the effect of the electrification level on the breakup time, can be observed only qualitatively given their dependence on the amplitude of the initial perturbation. Since the excitation is indirectly imposed, the transfer function between the excitation voltage on the piezoelectric tube and the initial perturbation undergone by jet cannot be accurately calculated. This kind of measurement can only be carried out by considering a direct transfer function, as is the case of Barbet (1997).

Two plots are given for each experimental condition: the non-dimensional droplet radius r_g/A versus the wavenumber k, and the non-dimensional charge transported by the droplets Q/Q_R, also versus k, where Q_R is the Rayleigh limit charge given by

$$Q_R = 8\pi\left(\varepsilon_o \gamma r_g^3\right)^{1/2}. \tag{4.1}$$

The influence of the liquid viscosity on the droplet size can be observed in figure 10, for a very similar value of the Taylor number Γ_o (approximately 0.1 in the first column), the Ohnesorge number C varying from 0.078 (bottom) to 0.271 (top). Consistently with all previous results in the field, the satellite radius decreases with increasing liquid viscosity. The radius reduction for $k = 0.7$ is roughly of the order of 30% from $C = 0.078$ to $C = 0.271$. As the viscosity increases, the discrepancies between experiments and the one dimensional model decrease since the flat velocity profile becomes a more realistic assumption.

The effect of Taylor number on the satellite radius is hardly noticeable (see figure 10), whereas an increase of the Ohnesorge number leads to a mild decrease of the satellite radius. Thus, although the liquid viscosity and electrical conductivity affect the satellite size (see figure 10), consistently with the published literature the excitation frequency is in reality the most effective way to gain a full control of the satellite droplet.

The non-dimensional charge of the main droplets is almost invariant with the wavelength. The agreement between experiment and theory is remarkably good (see figure 11). On the other hand, the non-dimensional satellite charge presents a minimum value for an intermediate viscosity as can be observed in plots (*e*) and (*h*) of figure 11, as a consequence of the competing effects of size reduction by viscosity and surface charge distribution on breakup: for the larger viscosity value (top row), the non-dimensional satellite charge is larger since Q_R is smaller corresponding to the size reduction (see (4.1)), while for the smaller viscosity the satellite size becomes larger and eventually acquires more charge during the breakup process.

The disagreement between theory and experiment is more noticeable the larger the Taylor number (last column of figures 10 and 11). This disagreement could be explained by the Coulombic explosions that may occur in the ligament appearing in the last stages of the breakup (see figure 12). These phenomena are more likely

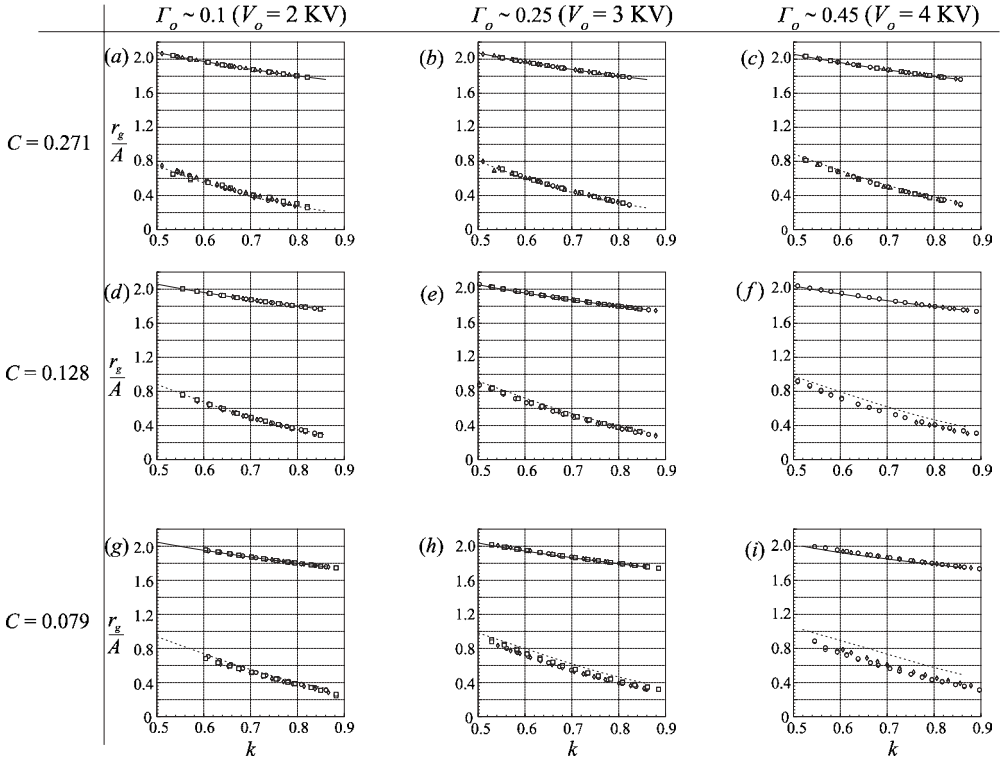

FIGURE 10. Non-dimensional values of the droplet radius r_g/A, being A the intact jet radius, versus the wavenumber k for increasing values of the Ohnesorge number C (bottom to top) and the Taylor number Γ_o (from left to right). The exact values of the Taylor number can be calculated from equation (3.2) using the jet voltage V_o. Lines correspond to numerical calculations (continuous to main droplets and dashed to satellites) whereas open symbols correspond to experimental data. In each plot, we have used different symbols for different experimental series under the same experimental conditions, for identification of the different experiments but these have no relevance for the comparison with theoretical predictions.

to appear the thinner the ligament, or, in other words, the smaller the viscosity and wavelength. Therefore, although Taylor number is relatively large in those cases (roughly $\Gamma_o \sim 0.4$), the agreement improves for the larger viscosity values (see plots (c) and (f) in figures 10 and 11).

4.1. *Some remarks and implications in electrospraying*

Whether this experimental model would resemble a real electrospray jet is a matter of discussion in terms of the relevant non-dimensional numbers which characterize the particular experimental conditions for an electrospray-emitted liquid jet. Clearly, the recent published literature points to a non-negligible voltage drop along any real electrosprayed jet (see Gañán-Calvo 1997, 1999; Gamero-Castaño & Hruby 2002), responsible of a tangential electric stress which thins the jet in the downstream direction. Nevertheless, the tangential-to-normal electric fields ratio on the jet surface is small (see Gañán-Calvo 1997, 1999), which was what led us to use the present model as a first approach to assess some features that may be observed in an electrospray. However, as can be observed from table 2, the errors in our model calculations underestimate significantly the experimental charge-to-mass ratio of Gamero-Castaño & Hruby (2002). Consequently, in those situations where the tangential electric field

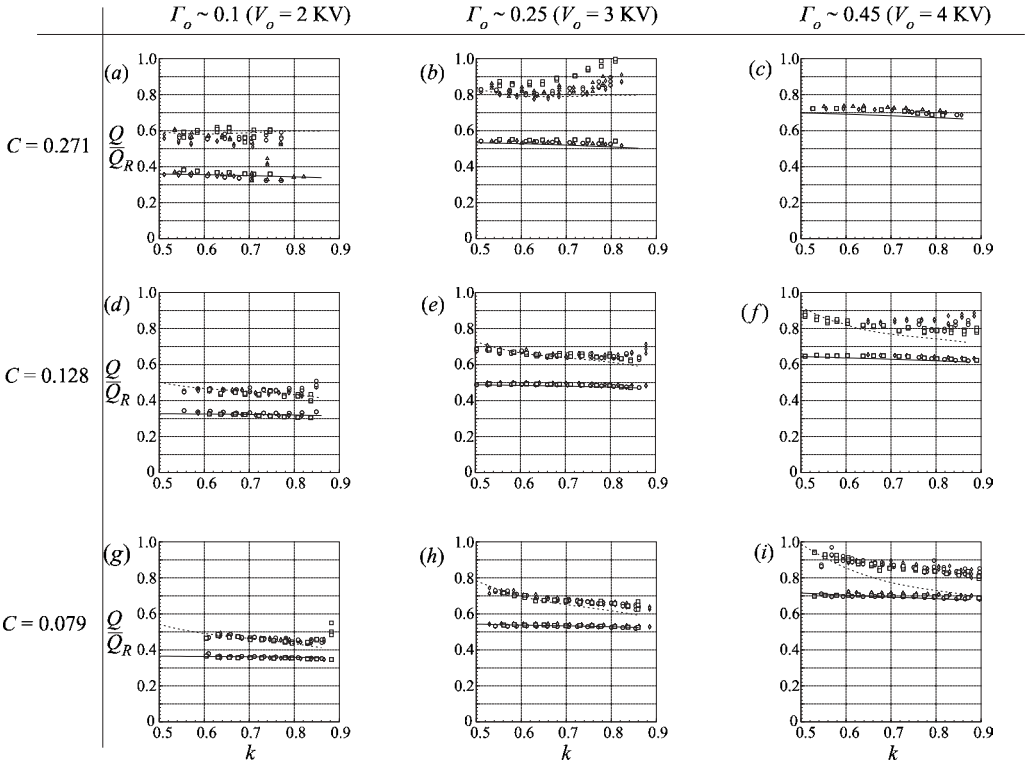

FIGURE 11. Non-dimensional values of the droplet charge Q/Q_R, being Q_R the Rayleigh limit charge, versus the wavenumber k for increasing values of the Ohnesorge number C (bottom to top) and the Taylor number Γ_o (from left to right). The exact values of the Taylor number can be calculated from equation (3.2) using the jet voltage V_o. Lines correspond to numerical calculations (continuous to main droplets and dashed to satellites) whereas open symbols correspond to experimental data. In each plot, we have used different symbols for different experimental series under the same experimental conditions, for identification of the different experiments but these have no relevance for comparison with theoretical predictions. In plot (*c*), the charge of the satellite droplets exceeds the Rayleigh limit value.

Solution	Q ($m^3\ s^{-1}$)	I (nA)	R_b (μm)	q/m (CK g^{-1})	q/m (model)	error (%)
TBP5	4,00E-11	41	0,57	0,9	0,654	27,3
TBP5	5,26E-11	48	0,65	0,78	0,572	26,7
TBP5	7,83E-11	57	0,81	0,64	0,493	22,9
TBP5	9,56E-11	62	0,88	0,57	0,459	19,4

TABLE 2. Experimental results of droplet charge-to-mass ratio (Gamero-Castaño & Hruby 2002) and predicted values from the present model. Q is the liquid flow rate, R_b is the jet radius at the breakup point, and q/m is the charge-to-mass ratio.

scales as that corresponding to the presence of the electrified conical meniscus (Taylor's field, see Gañán-Calvo 1997, 1999), our model would result in an unrealistic prediction of the jet breakup process.

When the issuing jet is sufficiently long compared to the general dimensions of the capillary feeding needle tip and the conical meniscus, the jet has a drastically

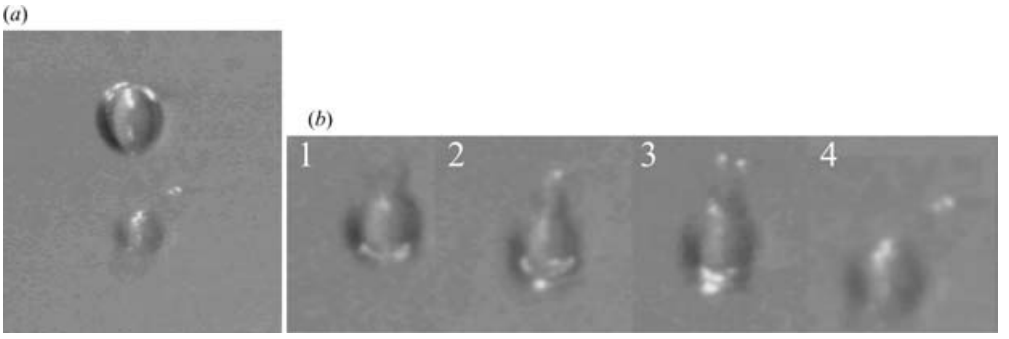

FIGURE 12. Pictures of the satellite disruption as a consequence of overcoming the Rayleigh limit charge, in the experimental conditions under which the theoretical model predicts this situation. (*a*): The satellite droplet in its relative position with the main droplet. (*b*) Four different stages of the satellite disruption and liquid ejection, where situation 4 corresponds to the satellite in (*a*). The blur in the pictures is due to the not exact periodicity of Coulombic emissions and to the large number of images superposed in every frame that we show in this figure. Note that the strobe frequency delivers a lot of very short light pulses every time the CCD shutter is open.

decreased tangential electric field in the breakup region. In these conditions, our model would be an appropriate predictive tool.

It is worth noting that the satellite charge passes the Rayleigh limit well before the main droplet, for quite moderate values of the Taylor number when the Ohnesorge number becomes sufficiently large (in our case, for Γ_o larger than about 0.4 and C larger than about 0.25). This means that the chance of observing Coulombic rupture of satellites becomes greater for rather moderate jet electrification levels if the liquid is sufficiently viscous or electrically conducting (see figure 11). Even though the scales are obviously not comparable, we suggest that these results are compatible with some recent experimental findings whose authors have hypothesized the role of satellite droplets in the appearance of single ions and ion clusters in electrospraying, in cases where Coulombic explosions were not expected for the main droplets. This is not to say that we observed ion/ion cluster emissions in our experiments. In fact, our jet sizes are orders of magnitude larger that those typical in an electrospray. However, we want to repeat here the result (numerical and experimental) that the satellite reaches the Rayleigh limit before the main droplet for an increasing electrification level. Since in addition the satellite is smaller and its evaporation velocity is significantly larger than that of the main droplet, in most cases the satellite will be prone to experience Coulomb explosions or a chain of explosions which would eventually yield ion/ion cluster emissions for rather moderate electrification levels, in cases where the role of the main droplets in these events is null.

In cases where our model could be applicable to actual electrosprays, it may allow to quantify the maximum electrification level for which Coulombic ruptures are absent as a function of the Ohnesorge number, which was out of the reach of prior linear analyses (e.g. Saville 1971*b*). Above this electrification level, one can expect a decrease of the quality of the spray (i.e. a less monodisperse aerosol) due to Coulombic explosions (Gomez & Tang 1994; Gamero-Castaño 1998). Since the Taylor number is significantly proportional to the jet radius in steady cone-jet electrospraying (Gañán-Calvo 1999), the flow rate range for which one has a fairly monodisperse aerosol is quite narrow in reality, consistent with the observations of Fernández de la Mora *et al.* (1990) and Chen, Pui & Kaufman (1995) and the conclusions that can

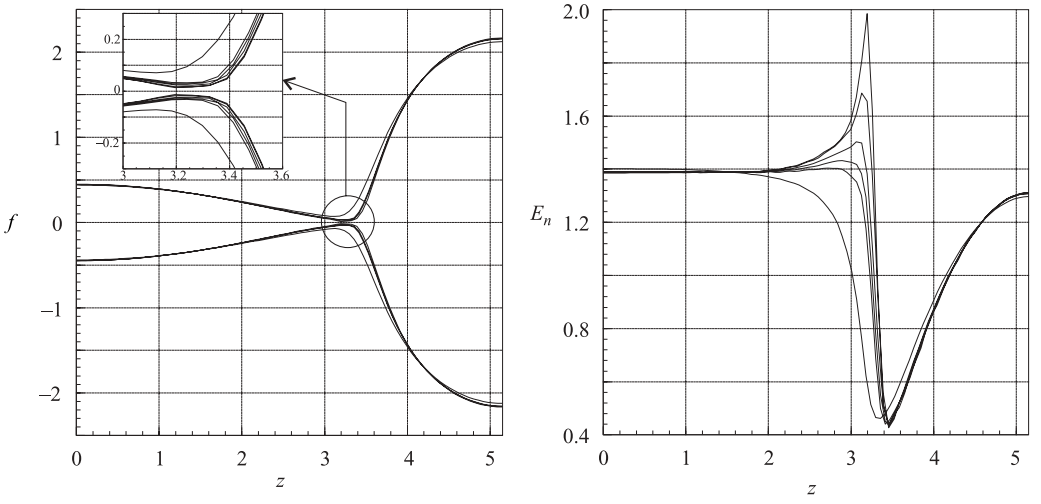

FIGURE 13. Last stages of the time evolution of the interface position (with a detail of the necking region) and normal electric field close to pinch-off. Recorded times $t =$ 12.7,12.80,12.81,12.82,12.83,12.833. $\lambda = 5.15, C = 0.128$ and $\Gamma_o = 0.389$.

be drawn from our model. Moreover, when the liquid viscosity is sufficiently large, the even, axisymmetric breakup regime may be intrinsically absent from the stable cone-jet electrospraying conditions, as shown by Hohman *et al.* (2001*a*, *b*).

4.2. *Some remarks on the accuracy of the electric field calculation in the pinch-off region*

We have learned that the last stages of the breakup are essential for determining the final values of the droplet charge. Consequently, the accuracy of the calculation of the surface charge density distribution in the pinch-off region may be crucial to achieving a good agreement between theory and experiments. As can be observed in figure 13, the electric field soars sharply at the point of minimum radius as the collapse of the interface approaches. In order to see in more detail how the different stresses on the jet surface evolve close to pinch-off at the necking region, figure 14 shows the ratio of the electrostatic pressure to the surface tension stress. We can observe in this figure that there is a clear lack of mechanical balance in favour of surface tension (since electric stress remains a mere 1% of the surface tension stress as $1/f_{min}$ soars), which precipitates the final neck pinching. Even though the electric field peak at the neck has a clear resemblance with the electrospraying phenomenon at the steady neck joining the cone and the jet, which in fact survives collapse by means of a local increase of the surface charge as a consequence of its quasi-equipotential nature (Gañán-Calvo 1997, 1999; Hartman *et al.* 2000), the final jet droplet pinch-off mechanism described here differs completely from the liquid ligament emission in electrospraying since electrostatic stresses are of paramount importance in this latter case at the cone-jet necking: while the electrospray cone-jet points in the direction of a strong potential gradient (the external electric field), our main and satellite liquid masses joined by a collapsing neck have the same potential, and as such the liquid contained in the necking region would not feel the influence of a strong axial field characteristic of electrospray. Thus, it will collapse almost exclusively through surface tension forces.

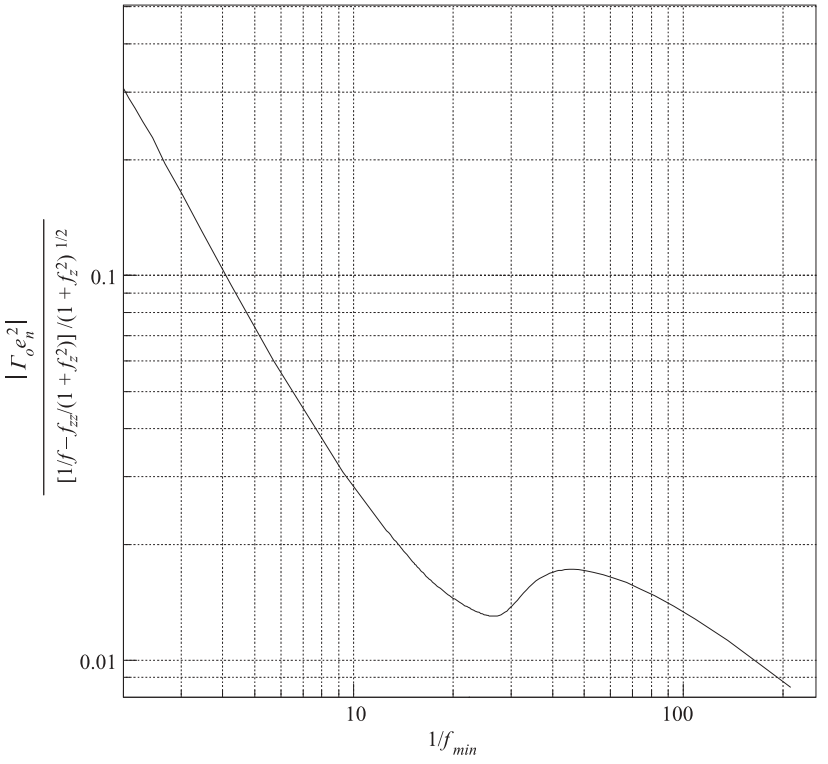

FIGURE 14. Evolution of the ratio of electric stresses to the surface tension stresses on the jet surface at the necking point (f_{min}), as a function of $1/f_{min}$; $\lambda = 5.15$, $C = 0.128$ and $\Gamma_o = 0.389$.

In addition, the pinch-off times, which scale as $(\rho f_{min}^3/\gamma)^{1/2}$, become arbitrarily small compared to the charge relaxation times ε/K close to collapse, which eventually invalidates any electrostatic process hypothesis at the pinching region. However, it can be observed in figure 15 that the dependence of the non-dimensional satellite charge before pinch-off on the minimum radius f_{min} becomes negligible for f_{min} below 1% of the intact jet radius in all our conditions, which makes irrelevant any further calculation refinement ahead of these very final stages. Here, it is necessary to point out that we have used a finite Fourier series formulation of the boundary element methods (Green's integral formulation) instead of the classical discretization of the contour domain into finite elements, since it appeared to be the best suited and smoothest scheme to reach as close as possible to the breakup point. Thus, the shapes plotted in figure 13 do no allow one to determine whether the resolution limit has been reached. We have performed a sensitivity analysis of the results (mainly the normal electric field in the neck vicinity, the resulting droplets volumes, and their eventual charges) on the number of terms of the series, when a 'minimum' radius (that we fix about 0.01) is reached. In other words, we fix our goal as reaching a certain minimum neck radius below which there is no change in the droplet volumes and charges under the most accurate conditions. Obviously, the smaller the radius goal, the larger the number of Fourier terms, and it is worth noting that the number of terms soars exponentially when we decrease the radius below 0.005, to the point that the code becomes computationally very inefficient. In fact, for a radius smaller than this goal (0.005), a better suited scheme should be developed. In conclusion, though, we must

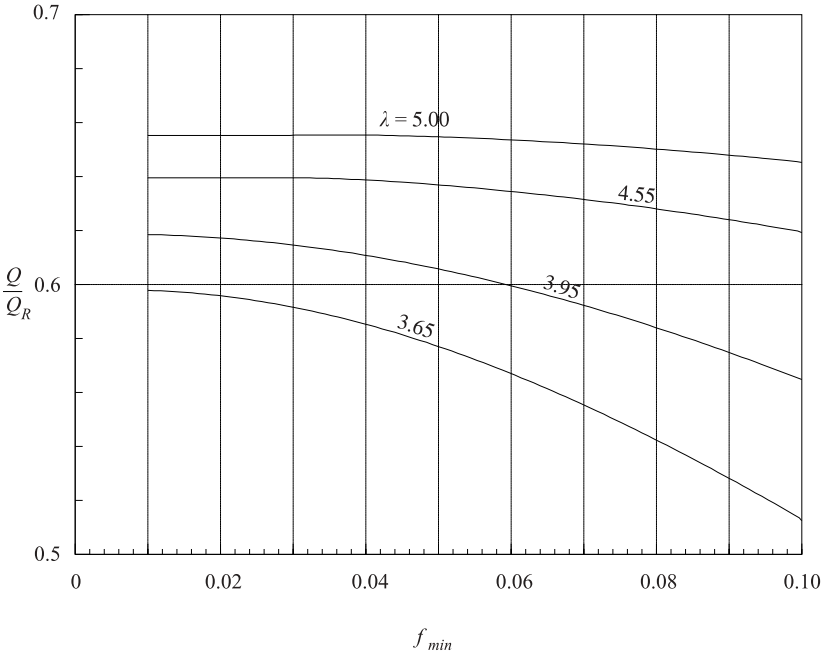

FIGURE 15. The non-dimensional satellite charge as a function of the minimum radius of the interface f_{min}; $C = 0.128$ and $\Gamma_o = 0.219$. Note that the charge becomes almost independent of the radius below $f_{min} \sim 0.01$ times the value of the intact radius.

emphasize again that the main and satellite droplet volumes and charges remain intact when the neck radius becomes smaller than about 0.01 (figure 15). Since these results (droplet volumes and charges) are the main targets of our study, our numerical scheme fulfils its objective.

5. Conclusions

In this note we present a large collection of experimental measurements of both droplet size and charge generated after charged liquid jet axisymmetric breakup. Both the main and satellite droplets are measured, and their size and charge are compared to the numerical results obtained from nonlinear simulations using an augmented one-dimensional model. The agreement between theoretical predictions and experiments is, in general, remarkably good except for the lower liquid viscosities and larger applied voltages. In these cases, the lack of agreement could be explained by the appearance of Coulombic ruptures and lateral liquid emissions from the thin ligament formed in the last stages of the breakup. In addition, the assumptions of a flat velocity profile and the domain slenderness in Lee's model become unrealistic for the lower viscosity and the shorter imposed breakup wavelength in our experiments. In any case, however, our results show that satellite droplets are particularly prone to undergoing Coulombic disruptions even in the case of very moderate jet surface charge values (or jet electrification levels) when the Ohnesorge number is higher than a certain value. We suggest that this finding could be, if not directly applicable, at least consistent with other recent findings that have pointed out the possible role of satellite droplets in the appearance of single ions and ions clusters in electrospraying, in situations where Coulombic explosions of the main droplets were not expected (e.g.

Gamero-Castaño 1998). However, the applicability of our model to real electrosprays would be viable only in cases where the jet length is sufficiently large compared to the electrified meniscus from which it issues or in other situations with a drastically reduced tangential electric field: for example, when the jet is forced to cross the electrode plate through an orifice (Gañan-Calvo 1998), and a voltage drop is applied between the liquid feeding tube and the orifice plate.

We are indebted to Mr Juan Jesús Borrero-García for his continuous assistance in the experimental data collection. J. L-H is indebted to Dr P. Atten for many ideas and suggestions during a stay at his laboratory at CNRS of Grenoble (France). We are also grateful for grants from Kraft Foods Inc. and the Ministry of Science and Technology of Spain, grant no. PB1996-1341.

REFERENCES

Ambravaneswaran, B., Phillips, S. D. & Basaran, O. A. 2000 Theoretical-analysis of dripping faucet. *Phys. Rev. Lett.* **85**, 5332–5335.

Ashgriz, N. & Mashayek, F. 1995 Temporal analysis of capillary jet breakup. *J. Fluid Mech.* **291**, 163–190.

Barbet, B. 1997 Stimulations electrohydynamique et thermique de jets de liquide conducteur. PhD thesis, Université Joseph Fourier-Grenoble-1.

Basset, A. B. 1894 Waves and jets in a viscous liquid. *Am. J. Maths* **16**, 93–110.

Brebbia, C. A. & Dominguez, J. 1989 *Boundary Elements. An Introductory Course*. Computational Mechanics Publications and McGraw-Hill.

Brenn, G. & Lackermeier, U. 1997 Drop formation from a vibrating orifice generator driven by modulated electrical signals. *Phys. Fluids* **9**, 3658–3669.

Chandrasekhar, S. 1961 *Hydrodynamic and Hydromagnetic Stability*, 1st Edn. Clarendon.

Chaudhary, K. C. & Maxworthy, T. 1980 Non linear capillary instability of a liquid jet. Part 2. Experiments on jet behaviour before droplet formation. *J. Fluid Mech.* **96**, 275–286.

Chaudhary, K. C. & Redekopp, L. G. 1980 Non linear capillary instability of a liquid jet. Part 1. Theory. *J. Fluid Mech.* **96**, 257–274.

Chen, A. U., Notz, P. K. & Basaran, O. A. 2002 Computational and experimental analysis of pinch-off and scaling. *Phys. Rev. Lett.* **88**, art. 174501.

Chen, D. R., Pui, D. Y. H. & Kaufman, S. L. 1995 Electrospraying of conducting liquids for monodisperse aerosol generation in the 4 nm to 1.8 μm diameter range. *J. Aerosol Sci.* **26**, 963–977.

Cloupeau, M. & Prunet-Foch, B. 1989 Electrostatic spraying of liquids in cone-jet mode. *J. Electrostatics* **22**, 135–159.

De Juan, L. & Fernandez de la Mora, J. 1997*a* Charge and size distributions of electrospray drops. *J. Colloid Interface Sci.* **186**, 280–293.

De Juan, L. & Fernandez de la Mora, J. 1997*b* Charge and size distributions of electrospray drops. *J. Colloid Interface Sci.* **195**, 267–268.

Donnelly, R. J. & Glaberson, W. 1966 Experiment on capillary instability of liquid jets. *Proc. R. Soc. Lond.* A **290**, 547–556.

Eggers, J. & Dupont, T. F. 1994 Drop formation in a one-dimensional approximation of the navier-stokes equations. *J. Fluid Mech.* **262**, 205–221.

Fernández de la Mora, J., Navascues, J., Fernández, F. & Rossell-Llompart, J. 1990 Generation of submicron monodisperse aerosols in electrosprays. *J. Aerosol Sci.* **21** (Suppl. 1), S673–S676.

Gañán-Calvo, A. M. 1997 Cone-jet analytical extension of taylor's electrostatic solution and the asymptotic universal scaling laws in electrospraying. *Phys. Rev. Lett.* **79**, 217–220.

Gañan-Calvo, A. M. 1998 Generation of steady liquid microthreads and micron-sized monodisperse sprays in gas streams. *Phys. Rev. Lett.* **80**, 285–288.

Gañán-Calvo, A. M. 1999 The surface charge in electrospraying: Its nature and its universal scaling law. *J. Aerosol Sci.* **30**, 863–872.

Gamero-Castaño, M. 1998 The transfer of ions and charged nanoparticles from solution to the gas phase electrospray. PhD thesis, University of Yale.

Gamero-Castaño, M. & Hruby, V. 2002 Electric measurements of charged sprays emitted by cone-jets. *J. Fluid Mech.* **459**, 245–276.

García, F. J. & Castellanos, A. 1994 One-dimensional models for slender axisymmetrical viscous-liquid jets. *Phys. Fluids* **6**, 2676–2689.

Goedde, E. F. & Yuen, M. C. 1970 Experiments on liquid jets instability. *J. Fluid Mech.* **40**, 495–511.

Gomez, A. & Tang, K. 1994 Charge and fission of droplets in electrostatic sprays. *Phys. Fluids* **6**, 404–414.

Green, A. E. 1976 On the nonlinear behavior of fluid jets. *Intl J. Engng Sci.* **14**, 49–63.

Hartman, R. P. A., Brunner, D. J., Camelot, D. M. A., Marijnissen, J. C. M. & Scarlet, B. 2000 Jet break-up in elelectrohydrodynamic atomization in the cone-jet mode. *J. Aerosol Sci.* **31**, 65–95.

Hohman, M. M., Shin, M., Rutledge, G. & Brenner, M. P. 2001*a* Electrospinning and electrically forced jets. I. Stability theory. *Phys. Fluids* **13**, 2201–2220.

Hohman, M. M., Shin, M., Rutledge, G. & Brenner, M. P. 2001*b* Electrospinning and electrically forced jets. II. Applications. *Phys. Fluids* **13**, 2221–2236.

Huebner, A. L. 1969 Disintegration of charged liquid jets. *J. Fluid Mech.* **38**, 679–688.

Keller, J. B., Rubinow, S. I. & Tu, Y. O. 1973 Spatial instability of a jet. *Phys. Fluids* **16**, 2052–2055.

Keunings, R. 1986 An algorithm for the simulation of transient viscoelastic flows with free surfaces. *J. Comput. Phys.* **62**, 199–220.

Lee, H. C. 1974 Drop formation in liquid jets. *IBM J. Res. Develop.* **18**, 364–369.

Lide, D. R. 1990 *Handbook of Chemistry and Physics*. CRC Press.

López-Herrera, J. M., Gañán-Calvo, A. M. & Perez-Saborid, M. 1999 One-dimensional simulation of the breakup of capillary jets of conducting liquids. application to e.h.d spraying. *J. Aerosol Sci.* **30**, 895–912.

Magarvey, R. H. & Outhouse, L. E. 1962 Note on the break-up of a charged liquid jet. *J. Fluid Mech.* **13**, 151–157.

Mansour, N. & Ludgren, T. S. 1990 Satellite formation in capillary jet breakup. *Phys. Fluids* A **2**, 1141–1144.

Melcher, J. R. 1963 *Field-Coupled Surface Waves*. M.I.T. Press.

Melcher, J. R. & Warren, E. P. 1971 Electrohydrodynamics current carrying semi-insulating jet. *J. Fluid Mech.* **47**, 127–143.

Mestel, A. J. 1994 Electrohydrodynamic stability of a slightly viscous jet. *J. Fluid Mech.* **274**, 93–113.

Mestel, A. J. 1996 Electrohydrodynamic stability of a highly viscous jet. *J. Fluid Mech.* **312**, 311–326.

Notz, P. K., Chen, A. U. & Basaran, O. A. 2001 Satellite drops: Unexpected dynamics and change of scaling during pinch-off. *Phys. Fluids* **13**, 549–552.

Rayleigh, Lord 1878 On the instability of jets. *Proc. Lond. Math. Soc.* **10**, 4–13.

Rosell-Llompart, J. & Fernandez de la Mora, J. 1994 Generation of monodisperse droplets 0.3 to 4 μm in diameter from electrified cone-jets of highly conducting and viscous liquids. *J. Aerosol Sci.* **25**, 1093–1119.

Saville, D. A. 1970 Electrhydrodynamic stability: Fluid cylinders in longitudinal electric fields. *Phys. Fluids* **13**, 2987–2994.

Saville, D. A. 1971*a* Electrohydrodynamic stability: Effects of charge relaxation at interface of a liquid jet. *J. Fluid Mech.* **48**, 815–827.

Saville, D. A. 1971*b* Stability of electrically charged viscous cylinders. *Phys. Fluids* **14**, 1095–1099.

Setiawan, E. R. & Heister, S. D. 1997 Nonlinear modeling of an infinite electrified jet. *J. Electrostatics* **42**, 243–257.

Sterling, A. M. & Sleicher, C. A. 1975 The instability of capillary jets. *J. Fluid Mech.* **68**, 477–495.

Tomotika, S. 1935 On the stability of a cylindrical thread of a viscous liquid surrounded by another viscous fluid. *Proc. R. Soc. Lond.* A **150**, 322.

Weber, V. C. 1931 Zum zerfall eines flüssigkeitsstrahles. *Z. Angew. Math. Mech.* **11**, 136–155.

Wilkes, E. D., Phillips, S. D. & Basaran, O. A. 1999 Computational and experimental analysis of dynamics of drop formation. *Phys. Fluids* **11**, 3577–3598.

Yildirim, O. E. & Basaran, O. A. 2001 Deformation and breakup of stretching briges of newtonian and shear-thinning liquids: Comparison of one- and two-dimensional models. *Chem. Engng Sci.* **56**, 211–233.

Yuen, M. C. 1968 Nonlinear stability of a liquid jet. *J. Fluid Mech.* **33**, 151–163.

Zeleny, J. 1917 Instability of electrified liquid surfaces. *Phys. Rev.* **10**, 1–6.

Zhang, X. & Basaran, O. A. 1996 Dynamics of drop formation from a capillary in the presence of an electric field. *J. Fluid Mech.* **326**, 239–263.